New Journal of Physics
The open-access journal for physics

Attosecond control of optical waveforms

Takao Fuji[1], Jens Rauschenberger[1], Christoph Gohle[1], Alexander Apolonski[2,3], Thomas Udem[1], Vladislav S Yakovlev[2], Gabriel Tempea[4], Theodor W Hänsch[1] and Ferenc Krausz[1,2,5]

[1] Max-Planck-Institut für Quantenoptik, Hans-Kopfermann-Strasse 1, D-85748 Garching, Germany
[2] Department für Physik, Ludwig-Maximilians-Universität München, Am Coulombwall 1, D-85748 Garching, Germany
[3] Institute of Automation and Electrometry, Russian Academy of Science, 630090 Novosibirsk, Russia
[4] Femtolasers Produktions GmbH, Fernkorngasse 10, A-1100 Wien, Austria
[5] Institut für Photonik, Technische Universität Wien, Gusshausstrasse 27/387, A-1040 Wien, Austria
E-mail: tkf@mpq.mpg.de

New Journal of Physics **7** (2005) 116
Received 14 February 2005
Published 3 May 2005
Online at http://www.njp.org/
doi:10.1088/1367-2630/7/1/116

Abstract. A new, monolithic scheme for stabilizing the phase between the carrier wave and the envelope (CE phase) in a train of few-cycle laser pulses is demonstrated. Self-phase modulation and second-harmonic generation or difference-frequency generation in a single periodically poled lithium niobate crystal, that transmits the main laser beam, allows for the CE-phase locking directly in the usable output. The monolithic scheme obviates the need for splitting off a fraction of the laser output for CE-phase control, coupling into microstructured fibre, as well as separation and recombination of spectral components. As a result, the CE-phase error integrated over the spectral range of 0.2 mHz–35 MHz is as small as $0.016\times 2\pi$ rad. This implies that the phase of the field oscillations ($\lambda \sim 830$ nm) with respect to the pulse peak is locked to within 44 attoseconds, resulting in optical waveform control with subhundred attosecond fidelity for the first time.

PII: S1367-2630(05)94740-X

Contents

1. Introduction 2
2. Experimental setup 3
3. Phase stabilization with the monolithic device 6
4. Pulse compression after phase stabilization 8
5. Conclusion 9
Acknowledgments 9
References 9

1. Introduction

Controlling the carrier-envelope (CE) phase of few-cycle light pulses is a key prerequisite for the reproducible generation of subfemtosecond XUV/soft-x-ray pulses used for pumping or probing the electron dynamics deep in the interior of atoms and molecules. In the first proof-of-concept experiments, intense phase-controlled few-cycle laser pulses [1, 2] were used to produce isolated 250 attosecond (as) pulses at photon energies near 100 eV [3]. Access to a wide range of electronic dynamics in core shells requires shorter and more energetic x-ray pulses. One of the major preconditions for their generation is the availability of intense few-cycle laser pulses, in which the timing of the field oscillations with respect to the pulse peak is controlled with an accuracy of the order of 100 as or better.

At present, the most widely used technique for stabilizing the CE offset frequency, f_{CEO}, the frequency at which the CE phase reproduces itself in the pulse train delivered by a mode-locked laser, is to measure the interference beat signal between the high-frequency and the second harmonic of the low-frequency spectral components of an octave-spanning spectrum and phase-lock this beat signal to a reference clock [4]–[8]. This scheme has been termed the f-to-2f method and relies on an alignment-sensitive interferometric apparatus. It uses an auxiliary beam branched off the main laser beam so that relative phase fluctuations or drifts between the two branches compromise the achievable CE-phase stability. Hence, any phase jitter accumulating between the laser output and the output of the phase control setup appears in the usable laser output, even if the electronic phase-locked loop works perfectly. In addition, the auxiliary setup for CE-phase stabilization introduces excessive dispersion, preventing the broadband output from being compressed to a few-cycle pulse. Recently, CE-phase stabilization with quantum interference control [9] by use of a single semiconductor has been demonstrated. However, a microstructured fibre is still necessary for this method and beam splitting before the fibre cannot be avoided for practical use. Alternatively, self-stabilization of the CE-phase by use of difference-frequency generation (DFG), which provides an intrinsically phase-stabilized signal ($f_{\mathrm{CEO}} = 0$), is possible, yet, the resulting pulse train is weak and located in a shifted wavelength region [10, 11].

In this paper, we demonstrate a scheme that allows for CE-phase stabilization directly in the usable laser output, resulting in a 70 MHz, 6 fs pulse train with a CE timing jitter of less than 50 as accumulated within 75 min. When the peak intensity of a pulse and the nonlinearity in a frequency-mixing crystal are large enough, both second-order nonlinear frequency mixing (second-harmonic generation (SHG) or DFG) and self-phase modulation (SPM) occur at the

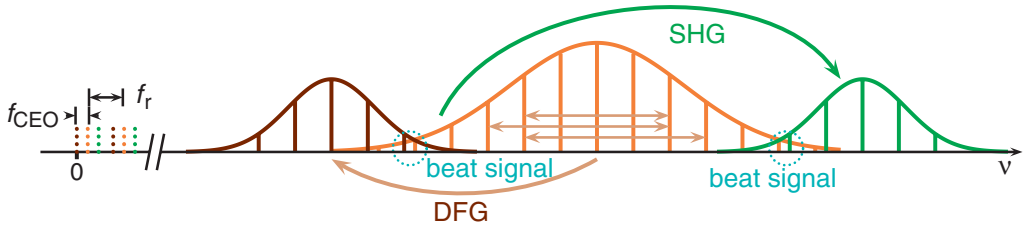

Figure 1. Principle of f_{CEO} detection: two additional frequency combs, $f_k = kf_r$ and $f_m = mf_r + 2f_{CEO}$, are created in a nonlinear crystal by DFG and SHG, respectively. The frequency comb of the seed laser $f_n = nf_r + f_{CEO}$, which is spectrally broadened by SPM, is located between the DFG and SHG combs. With k, n and m being integers, the combs partially overlap to produce heterodyne beat notes at f_{CEO}.

same time. In regions of spectral overlap, a CE offset (CEO) beat between these two waves at f_{CEO} was observed in thin BBO [12] and ZnO [13] crystals. In this work, we tightly focus few-cycle pulses from a Ti : sapphire oscillator with a repetition rate $f_r = 70$ MHz into a highly nonlinear magnesium-oxide-doped periodically poled lithium niobate (PP-MgO : LN) crystal to induce SPM and SHG/DFG (see figure 1). Owing to the enhanced nonlinear interaction and an improved spatial overlap between the two waves (due to the absence of walk-off effects), the interferometric beat signal emerging at f_{CEO} in the region of spectral overlap is strong enough for reliable CE-phase locking.

Further important differences from previous CE-phase locking schemes include the CEO beat signal emerging outside the original laser spectrum (allowing its easy isolation) and moderate dispersion in the nonlinear medium (allowing recompression of the transmitted laser pulses). The implications are numerous and far reaching: (i) full laser power is used for inducing the nonlinear processes in a monolithic device, (ii) almost the entire laser power is available for application such as probing CE-phase-dependent nonlinear processes or amplifier seeding, (iii) absence of a microstructured fibre avoids instabilities (amplitude and CE phase) associated with coupling into its tiny core, and (iv) most importantly, the CE phase is controlled directly in the beam that is used for applications.

2. Experimental setup

The Ti : sapphire oscillator is based on the all-chirped-mirror oscillator described in [14]. The schematic representation of the cavity is shown in figure 2(a). It generates pulses with a spectrum extending from 660 to 1000 nm at −10 dB below its maximum (figure 2(b)). The ultra-broadband chirped mirrors used for dispersion control inside and outside the cavity exhibit tailored dispersion over 620–1100 nm and were manufactured with a Helios sputtering system by Leybold Optics. The overall round-trip group delay dispersion of the laser resonator is shown in figure 2(b). The average output power of the oscillator is 420 mW at 5.0 W pump power and 70 MHz repetition rate. The spatial profile of the beam is approximately Gaussian.

The experimental setup for the phase-stabilization scheme is shown in figure 3. A pair of extracavity chirped mirrors compensates for the dispersion of the output substrate and compresses

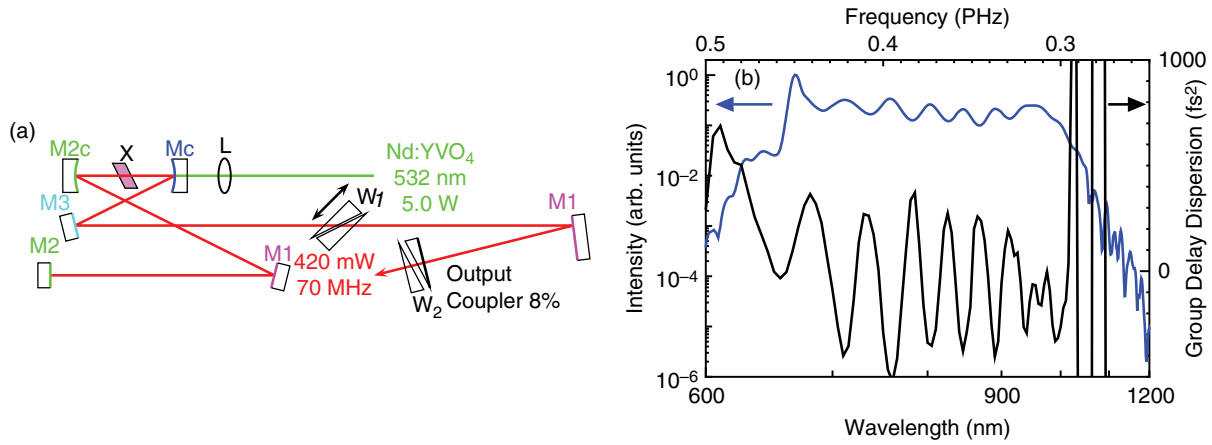

Figure 2. (a) The schematic representation of the broadband Ti : sapphire oscillator. X, Ti : sapphire crystal ($t = 2.6$ mm); Mc/M2c, 50 mm ROC folding mirror; M1–M3, chirped mirrors; and L, incoupling lens. The wedged plates inside the laser cavity (W_1) allow the controlling of CEO frequency (f_{CEO}), while extra-cavity wedges (W_2) shift the CE-phase. (b) Spectrum generated by the oscillator (blue curve), measured with a scanning monochromator (Ando, AQ-6315A) and net intracavity group-delay dispersion (GDD, black curve).

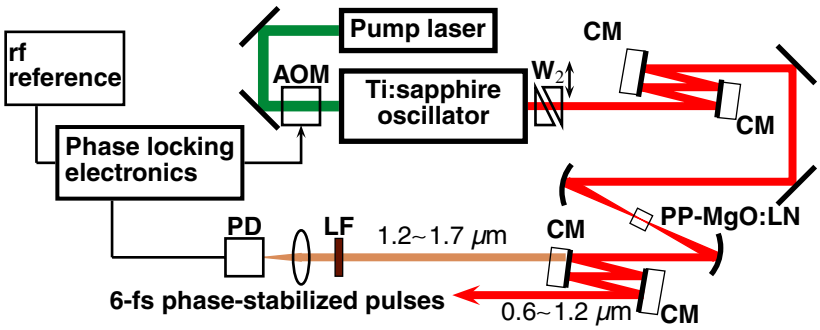

Figure 3. Experimental realization of the monolithic CE-phase stabilization scheme. W_2, fused silica-wedged plate that may be used for control of the CE-phase and fine adjustment of the chirp. CM, chirped mirror; LF, long-pass filter (cutoff 1400 nm); PD, InGaAs photodiode (NewFocus, 1811-FC), phase-locking electronics (MenloSystems); rf reference, signal generator (Marconi, 2022D: operated at 12.5 MHz); and AOM, acousto-optic modulator.

the pulses to ~6 fs duration. They are focused into a 2 mm-long PP-MgO : LN crystal (HC Photonics) with a poling period of 11.21 μm, optimized for type 0 ($e + e \rightarrow e$) DFG between 620 and 1000 nm. The crystal is operated at room temperature. The spot size inside the crystal, w_0, is ~15 μm. As shown in figure 3, one of the chirped mirrors also acts as a dichroic beam splitter after the crystal. It reflects the fundamental spectrum and transmits the infrared components of the beam at >1250 nm, which emerge from the nonlinear interactions in the PP-MgO : LN crystal. The transmitted beam is passed through a long-pass filter (1400 nm cutoff) and detected by an InGaAs photo diode (New Focus, Model 1811-FC).

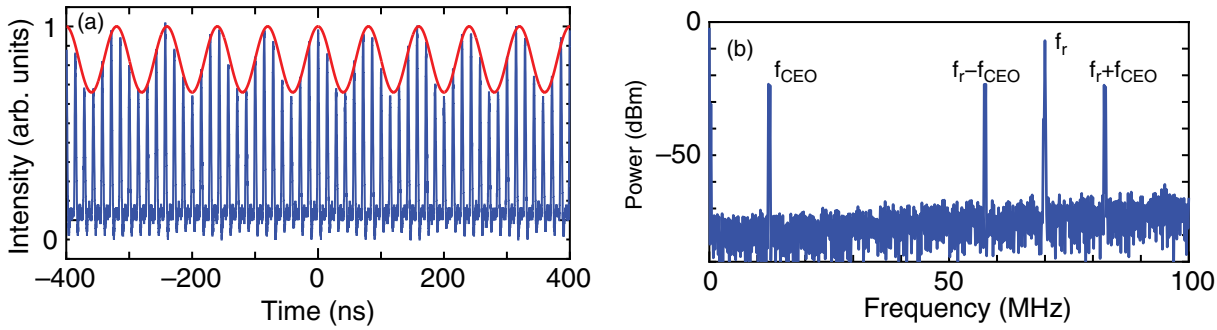

Figure 4. (a) A pulse train from the nonlinear crystal filtered in the wavelength range of longer than 1400 nm is modulated at f_{CEO} (red curve) and monitored with a digital oscilloscope (Tektronix, TDS7104). (b) rf spectrum of the same signal measured with a spectrum analyser (Agilent E4401B). Resolution bandwidth is 100 kHz.

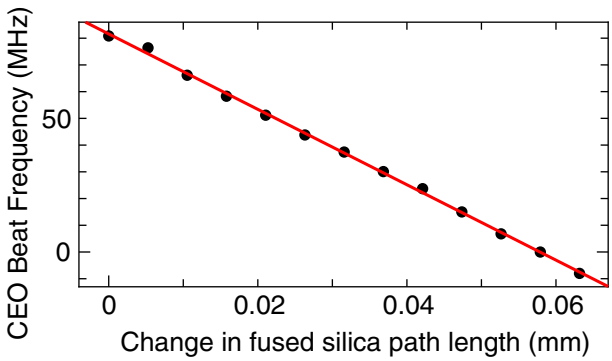

Figure 5. Measured CEO beat signal versus change in round-trip path length through the intracavity-fused silica wedges.

The signal of this photo detector is shown in figure 4. In the time domain, the detected pulse train is modulated with the CEO frequency (figure 4(a)), generating corresponding side bands to the repetition rate and its harmonics in the frequency domain (figure 4(b)). By optimizing the chirp of the pulses in the crystal by means of wedged-fused silica plates (W_2) and negatively chirped mirrors outside the cavity, a signal-to-noise ratio (S/N) in excess of 55 dB in a resolution bandwidth of 100 kHz can be achieved. This permits routine locking of the CEO frequency to a reference with the servo loop system described in [8]. A beat signal showing a comparable S/N is observed at about 580 nm using the nonlinear crystal optimized for SHG (9.07 μm period). The beat frequency can be tuned with the wedged plates (W_1) inside the cavity [8, 12]. The fused-silica path length dependence of the beat frequency (figure 5) is linearly fit as $f(\delta z) = f_0 - 20\,\mathrm{mm}^{-1}\, f_r\, \delta z$, where f is the beat frequency, δz the change in fused-silica path length, f_0 the beat frequency at $\delta z = 0$ and f_r the repetition rate. The coefficient of the linear function ($20\,\mathrm{mm}^{-1}$) matches excellently the one determined from the group and phase delay difference of fused silica, providing clear evidence for the origin of the observed beating.

Figure 6 shows the long-wavelength tail of the spectrum exiting the crystal. Newly generated spectral components in the wavelength region of longer than 1150 nm are clearly visible in the near infrared region when the crystal is translated into the focal region of the laser beam. The

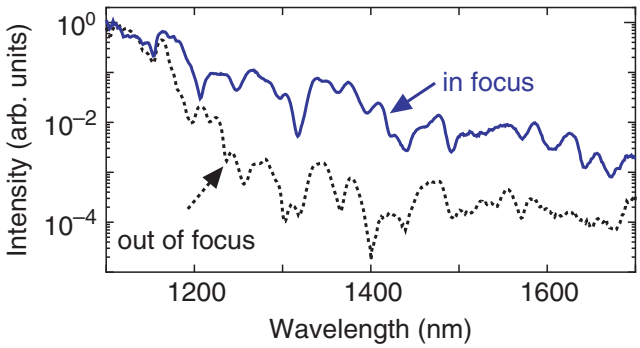

Figure 6. The long-wavelength tail of the laser spectrum exiting from the nonlinear crystal, measured with an optical spectrum analyser (Ando, AQ-6315A). The solid line shows the optimized spectrum, whereas the dotted line depicts it with the crystal shifted out of focus, for reference.

main part of the spectrum, from 600 to 1150 nm, does not change in shape. The infrared light is attributed to SPM and phase-matched DFG. A nonlinear CE phase shift due to SPM inside the PP-MgO : LN crystal estimated at $0.012 \times 2\pi$ radians by numerical simulations is present. Fluctuations of this phase shift, however, does not compromise the stability of the CE phase in the output beam, because it is fully compensated by the servo loop. This is in contrast with the conventional scheme, where the SPM-induced phase noise in the auxiliary beam for phase stabilization is written onto the main laser output and cannot be compensated by the servo loop. The beating between the DFG and SPM (SHG and SPM) is observed at $\lambda > 1350$ nm ($\lambda \cong 580$ nm).

3. Phase stabilization with the monolithic device

The spatial and temporal matching of the waves interfering in a monolithic device is expected to improve CE-phase control over that provided by conventional schemes. To test the performance, the laser beam that emerges from our setup in figure 3 is focused onto another PP-MgO : LN crystal for a second independent CE-phase measurement. To our knowledge, such an out-of-loop characterization of CE phase stabilization without fibre broadening [15]–[18] has not been performed so far. This out-of-loop signal provides an upper limit to the stability of the CE phase, as phase noise added by the locking electronics and both the in-loop and out-of-loop CE-phase detection systems is included. Since the chirped mirror used as a dichroic mirror has some reflectivity around 600 nm, the beat signal generated in the first crystal can be still observed at the second detection system, rendering an out-of-loop measurement with SHG phase-matching impossible. On the other hand, in the near-infrared region (>1350 nm), the beat signal generated in the first crystal has completely disappeared at the second f_{CEO} detector after several reflections off the chirped mirrors. Therefore, the out-of-loop measurement is performed only with the near-infrared output. We measured the relative phase of the f_{CEO} frequency as detected by the two independent f_{CEO} detectors. To this end, the first detector was used to lock the f_{CEO} beat to an rf reference at 12.5 MHz and the signal of the second f_{CEO} detector was compared to the same reference. Slow drifts of the CE-phase in the spectral range of 0.2 mHz–1 Hz were detected by recording the phase error between the reference signal at 12.5 MHz and the out-of-loop beat signal

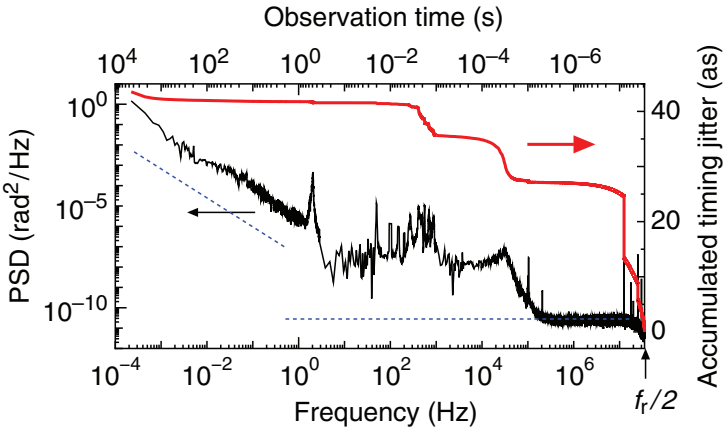

Figure 7. Out-of-loop two-sided phase-noise power spectral density (PSD), $S_\phi(\nu)$ and integrated CE timing jitter. The dotted line shows the noise floor of the photo detector and the vector voltmeter for low frequencies. The large peaks in the high frequency region (12.5, 17.5, 20, 25, 30 MHz) are originated from rf pick up.

with a vector voltmeter (Hewlett Packard, HP8405A). For observing the fast jitter (frequency range 1 Hz–35 MHz) of the CE-phase, the signal of the second f_{CEO} detector was monitored by a digital oscilloscope. For the intermediate frequency region (frequency range 1 mHz–10 Hz), the beat signal was electronically mixed with the reference and the dc signal recorded with a voltmeter. The oscilloscope and the reference frequency generator were both referenced to a high-quality quartz clock (Oscilloquartz, OCXO8607). This procedure permits us to accurately measure the temporal variation of the CE-phase, $\phi(t)$. The two-sided power spectrum of phase fluctuations, $S_\phi(\nu)\,\mathrm{d}\nu$, which is the absolute square of the Fourier transform of the CE phase as derived from the recorded time series, is shown in figure 7. The lowest resolved frequency component is given by the inverse of the observation time of 75 min. Since the CE phase advance is only measurable when a pulse arrives (figure 4(a)), the pulse train samples the f_{CEO} signal and the largest possible Fourier spectrum of the jitter of the CE phase extends to $f_{\mathrm{r}}/2$ according to the Nyquist theorem. The accumulated timing jitter ΔT_{rms} as a function of the observation time τ_{obs},

$$\Delta T_{\mathrm{rms}}(\tau_{\mathrm{obs}}) = \frac{\lambda_{\mathrm{C}}}{2\pi c}\Delta\phi_{\mathrm{rms}}(\tau_{\mathrm{obs}}) = \frac{\lambda_{\mathrm{C}}}{2\pi c}\sqrt{2\int_{1/\tau_{\mathrm{obs}}}^{f_{\mathrm{r}}/2} S_\phi(\nu)\,\mathrm{d}\nu}, \tag{1}$$

is also shown in figure 7. $\Delta\phi_{\mathrm{rms}}(\tau_{\mathrm{obs}})$ denotes the integrated CE phase error and λ_{C} the centre wavelength of the pulses. The phase error integrated from $f_{\mathrm{r}}/2 = 35$ MHz to 0.2 mHz is $0.016 \times 2\pi$ rad, or 44 as of timing jitter at the centre wavelength of ~830 nm. For frequencies above 200 kHz, the CE phase noise is lower than our current noise floor set by the photo detector. Nevertheless, we can set an upper limit to the CE-phase noise in the accessed spectral range from these data.

By use of a conventional f-to-$2f$ scheme, phase-stabilization with very small timing jitter was also demonstrated earlier [19, 20]. However, only the phase stability of a single phase locked loop was measured. Such an in-loop measurement of the timing jitter can be used only to determine the effectiveness of the stabilization circuitry, rather than the constancy of the CE-phase in the laser output [21, 22]. Two other reports show timing jitter measurements from two separate

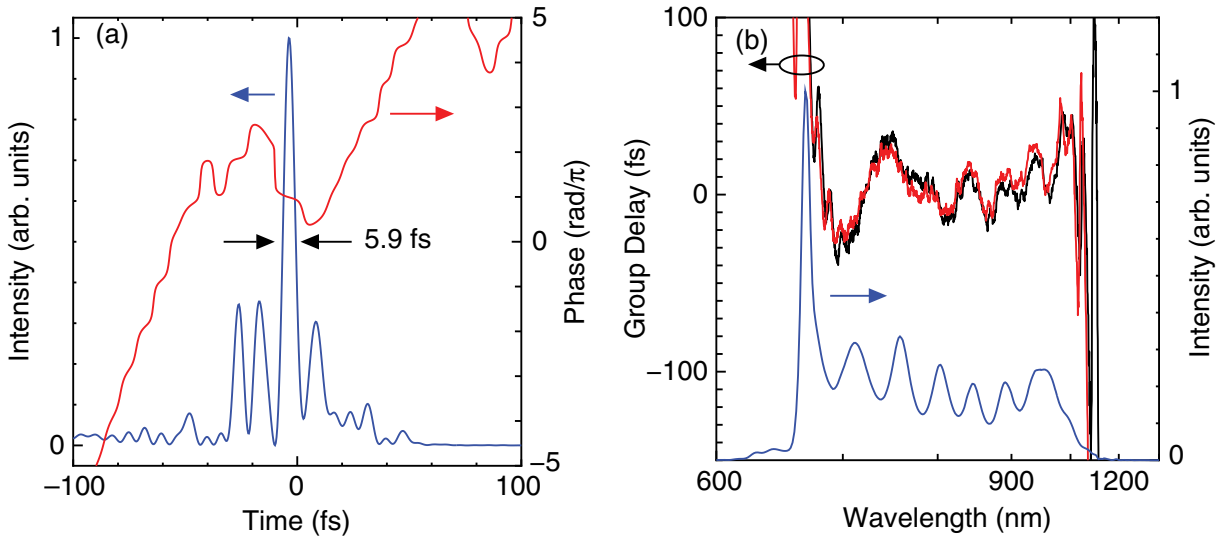

Figure 8. (a) Temporal profile of the output pulses of the phase-stabilized system (passing through the 2 mm length PP-MgO : LN and compressed with chirped mirrors), as retrieved from a SPIDER measurement. The full-width at half-maximum of the intensity profile is 5.9 fs. (b) Group delay (black curve) and spectrum (blue curve, linear scale) of the pulses. The group delay when the beam is not focused on the crystal is also shown as a red curve.

phase locking loops (out-of-loop). In [22], a timing jitter of <100 as was achieved. However, the observation time in this study was too short (4 ms) to be relevant for attosecond spectroscopy where signal accumulation over many laser pulses (several minutes) is necessary. Another report [21] claims approximately 310 as timing jitter in a 0.9765 mHz–102 kHz frequency band. With the same integration time (from 102.4 kHz to 0.9765 mHz) as used in [21], our integrated phase error would be $0.012 \times 2\pi$ rad, corresponding to 34 as of timing jitter and constituting a one-order of magnitude improvement. The most significant difference appears in the low-frequency region (<10 mHz), where amplitude-to-phase coupling in the microstructured fibre is dominant.

4. Pulse compression after phase stabilization

In the present system, the mirror compressor and the crystal have a combined loss of $\sim$30% due to the mirror coating quality, the photorefractive effect in the crystal, etc. The photo refractive effect alone is responsible for more than 20% loss. This loss can be avoided by heating the crystal. The dispersion of the crystal may be compensated by chirped mirrors as shown in figure 8. The pulse energy passed through the compressor is 300 mW, $\sim$4.3 nJ. The compressed pulses have been characterized with a broadband SPIDER apparatus [23] with the results being summarized in figure 8. The absence of serious phase distortions from nonlinear frequency mixing is verified by comparing the SPIDER results with the crystal being in focus and out of focus. The measurements yielded a pulse width of 5.9 fs, whereas the transform-limited pulse width is 4.8 fs. Deviation from this ideal case is mainly attributed to residual cubic dispersion of the cavity GDD (figure 2(b)) at short wavelengths. Its suppression with an improved mirror design will reduce the fractional energy of satellite pulses and compress the main pulse.

5. Conclusion

In conclusion, we have demonstrated a simple, highly efficient monolithic scheme for direct CE-phase stabilization of a mode-locked laser delivering few-cycle pulses. In the first implementation of the new concept, CE phase-locked, 5.9 fs pulses with several nanojoules of pulse energy have been produced at a repetition rate of 70 MHz with unprecedented long-term reproducibility of the generated few-cycle waveforms. The scheme can be adapted to lasers operating in other wavelength regions. The demonstrated technology may be a key to pushing the frontier of attosecond science to the atomic timescale.

Acknowledgments

We gratefully acknowledge support from the FWF (Austria) through grants Z63 and P15382, and the European Community's Human Potential Programs under contract MRTN-CT-2003-50138 (XTRA).

References

[1] Baltuška A *et al* 2003 *Nature* **421** 611
[2] Baltuška A, Uiberacker M, Goulielmakis E, Kienberger R, Yakovlev V S, Udem Th, Hänsch T W and Krausz F 2003 *IEEE J. Sel. Top. Quantum Electron.* **9** 972
[3] Kienberger R *et al* 2004 *Nature* **427** 817
[4] Reichert J, Holzwarth R, Udem Th and Hänsch T W 1999 *Opt. Commun.* **172** 59
[5] Telle H R, Steinmeyer G, Dunlop A E, Stenger J, Sutter D H and Keller U 1999 *Appl. Phys.* B **69** 327
[6] Jones D J, Diddams S A, Ranka J K, Stentz A, Windeler R S, Hall J L and Cundiff S T 2000 *Science* **288** 635
[7] Holzwarth R, Udem Th, Hänsch T W, Knight J C, Wadsworth W J and Russell P St J 2000 *Phys. Rev. Lett.* **85** 2264
[8] Poppe A, Holzwarth R, Apolonski A, Tempea G, Spielmann Ch, Hänsch T W and Krausz F 2001 *Appl. Phys.* B **72** 373
[9] Roos P A, Li X, Smith R P, Pipis J A, Fortier T M and Cundiff S T 2005 *Opt. Lett.* **30** in press
[10] Zimmermann M, Gohle C, Holzwarth R, Udem T, and Hänsch T W 2004 *Opt. Lett.* **29** 310
[11] Fuji T, Apolonski A and Krausz F 2004 *Opt. Lett.* **29** 632
[12] Apolonski A, Poppe A, Tempea G, Spielmann Ch, Udem Th, Holzwarth R, Hänsch T W and Krausz F 2000 *Phys. Rev. Lett.* **85** 740
[13] Mücke O D, Tritschler T, Wegener M, Morgner U and Kärtner F X 2002 *Opt. Lett.* **27** 2127
[14] Fuji T, Unterhuber A, Yakovlev V S, Tempea G, Stingl A, Krausz F and Drexler W 2003 *Appl. Phys.* B **77** 125
[15] Morgner U, Ell R, Metzler G, Schibli T R, Kärtner F X, Fujimoto J G, Haus H A and Ippen E P 2001 *Phys. Rev. Lett.* **86** 5462
[16] Ramond T M, Diddams S A, Hollberg L and Bartels A 2002 *Opt. Lett.* **27** 1842
[17] Fortier T M, Jones D J and Cundiff S T 2003 *Opt. Lett.* **28** 2198
[18] Matos L, Kuzucu O, Schibli T R, Kim J, Ippen E P, Kleppner D and Kärtner F X 2004 *Opt. Lett.* **29** 1683
[19] Helbing F W, Steinmeyer G and Keller U 2003 *IEEE J. Sel. Top. Quantum Electron.* **9** 1030
[20] Helbing F W, Steinmeyer G, Stenger J, Telle H R and Keller U 2002 *Appl. Phys.* B **74** S35
[21] Fortier T M, Jones D J, Ye J and Cundiff S T 2003 *IEEE J. Sel. Top. Quantum Electron.* **9** 1002
[22] Witte S, Zinkstok R T, Hogervorst W and Eikema K S E 2004 *Appl. Phys.* B **78** 5
[23] Iaconis C and Walmsley I A 1999 *IEEE J. Quantum Electron.* **35** 501